J. Fluid Mech. (1993), vol. 255, pp. 683–705

Development of three-dimensional, streamwise-periodic flows in mixed-convection heat transfer

By S. RAVI SANKAR[1], P. A. J. MEES[2] AND K. NANDAKUMAR[2]

[1]Department of Chemical Engineering, Monash University, Australia

[2]Department of Chemical Engineering, University of Alberta, Edmonton, Alberta, Canada, T6G 2G6

(Received 24 November 1992 and in revised form 12 May 1993)

The three-dimensional, parabolized form of the coupled equations of motion and energy are solved to study the development of mixed-convection heat transfer in the entrance region of horizontal square ducts. The specific problem considered here is that of axially uniform heat flux and peripherally uniform temperature with parabolic inlet profile and uniform inlet temperature in a square cross-section. Previous studies have been confined mostly to two-dimensional flows in the fully developed region. Recent two-dimensional calculations have indicated the existence of multiple steady-state solutions in the fully developed region with two- and four-cell flow structure. Present three-dimensional calculations, carried over the whole entrance length and the full cross-section, indicate the evolutionary path that lead to such two-dimensional flows. Furthermore they shed new light on the nature of flows in regions where all known two-dimensional solutions become unstable in some manner. For low Grashof numbers and $Pr = 0.73$ the secondary velocities develop into an axially invariant state with two counter-rotating vortices. For Grashof numbers above 2.2×10^5 the inlet profiles evolve into a state with a four-cell secondary flow structure. As in a related problem of flow in a curved channel (Winters 1987; Bara *et al.* 1992), the two-dimensional, four-cell solutions are found to be unstable to asymmetric perturbations. Such perturbations trigger a new, *streamwise-periodic* mode which is sustained over long lengths in the flow direction. For Grashof numbers above 5.6×10^5 axially invariant two-cell solutions reappear. Some of the three-dimensional solutions corresponding to the streamwise periodic mode lack the reflective symmetry about the vertical centreline and hence these flows occur with multiplicity of two.

1. Introduction

Fully developed, two-dimensional mixed-convection heat transfer in horizontal ducts of rectangular and circular cross-sections has been studied quite extensively since the early work of Morton (1959). Hence the problem has come to be known as the Morton problem. The extensive literature is due, in part, to the importance of this mechanism in heat exchangers. In addition it serves as a model problem of an open channel flow to study the physics of flow transitions. The nonlinear coupling between the momentum and energy equations results in a complex bifurcation structure of the

two-dimensional solutions. Most of the early works did not, of course, take account of or explore these features.

Experimental results are presented by Bergles & Simonds (1971) for the case of uniform wall flux boundary, by Yousef & Tarasuk (1981) for the case of uniform wall temperature boundary and by Osborne & Incropera (1985) for the case of asymmetric heating. Early work revealed that the pressure-driven axial flow was superimposed with a secondary, buoyancy-driven flow consisting of two counter-rotating vortices. The first evidence of a transition to a four-cell secondary flow pattern was contained in the numerical work of Patankar, Ramadhyani & Sparrow (1978) for a circular tube with non-uniform peripheral heating. Chou & Hwang (1984) found a similar behaviour for a rectangular duct with uniform peripheral heating. Patankar *et al.* (1978) also showed that in the fully developed region, the flow and heat transfer characteristics depend only on a single dynamical parameter, viz. a modified Grashof number, and not separately on Reynolds and Rayleigh numbers. The continued interest in the problem is quite evident from the recent work of Van Dyke (1990), who extended the Stokes series solution of Morton (1959) to 31 terms with the aid of a computer. He examined the two-dimensional flows only in a circular cross-section and the multiplicity aspects were not investigated. Multiplicity features of such flows were first observed in our earlier works (Nandakumar, Masliyah & Law 1985; Fung, Nandakumar & Masliyah 1977). The complete bifurcation structure of the two-dimensional flows was revealed in a recent work by Nandakumar & Weinitschke (1991, hereinafter referred to as I).

The equations governing the laminar mixed-convection flow problem are similar to those of laminar flow in coiled ducts (the Dean problem). The flow features of the Dean problem in the fully developed domain have been examined by Dennis & Ng (1982) and Nandakumar & Masliyah (1982) for curved ducts of circular cross-section. Of particular interest are the recent theoretical work of Winters (1987) and experimental work of Bara, Nandakumar & Masliyah (1992) for a curved, rectangular geometry. Winters (1987) has presented a complete bifurcation picture of two-dimensional solutions. Bara *et al.* (1992) have experimentally verified the dual solutions and investigated the three-dimensional flow development leading to a fully developed state. One of the main results of these studies is that the *four-cell, two-dimensional solution is unstable to asymmetric perturbations* and that over a narrow window of Dean number, no stable two-dimensional solutions exist. A natural consequence is that the stability is transferred to a solution branch with a more complicated flow structure. Likely possibilities are those that break the translational symmetry giving rise to streamwise-periodic modes or travelling wave solutions. Purely time-periodic, two-dimensional motions that arise through a Hopf bifurcation are unlikely to be realized in any experiment as there is a predominant flow direction and hence any perturbation at a streamwise location will not only grow temporally but will also be convected downstream, *i.e.* we have a *convective instability* (Monkewitz 1990) as opposed to *absolute instability*. Ravi Sankar *et al.* (1988), in fact found that when a two-dimensional, four-cell flow is perturbed at a spatial location, the perturbation grows spatially in the downstream direction destroying the two-dimensional solution and replacing it with a streamwise-periodic, three-dimensional solution. In the present work we examine the occurrence of a similar phenomenon in laminar mixed-convection flow through horizontal straight ducts.

Entrance region (three-dimensional) mixed-convection flows have also been studied quite extensively. Briley (1971) considered an axially uniform flux condition in a square geometry and used this problem as a test of his proposed numerical

method, but did not present an extensive parametric study. The numerical method that he developed was based on the *parabolized* form of the equations of motion. Hieber & Sreenivasan (1974) considered a circular pipe with axially uniform wall temperature and a large-Prandtl-number fluid. Hishida, Nagano & Montesclaros (1982) re-examined that problem numerically after relaxing the large-Prandtl-number assumption and retaining the *elliptic* formulation. Their grid resolution is, however, quite coarse with only 26 point in the streamwise direction. Use of an iterative successive relaxation scheme also restricts the range of Grashof numbers over which reliable, converged results could be obtained. No attempt is made to compare the results of their elliptic formulation to those based on parabolized formulation.

Note that for the axially uniform wall temperature condition, as the fluid warms up to the wall temperature, the buoyancy effect decreases asymptotically with increasing axial position. As pointed out by Hieber & Sreenivasan (1974), the forced convection becomes the dominant mechanism far downstream of the tube and hence the final asymptotic development of the temperature field corresponds to that of the Graetz problem. The case of constant flux in the axial direction provides a *sustained* forcing along the entire length of the tube, thus making it similar to the Dean problem in a continuously coiled duct where a sustained centrifugal force is present along the length of the flow. For rectangular ducts the case of an axially and peripherally uniform flux condition has been considered by Abou-Ellail & Morcos (1983) while the bottom-heated case has been studied by Incropera & Schutt (1985) and Mahaney, Incropera & Ramadhyani (1987) using the *parabolized* form of the equations. Mahaney *et al.* (1987) suggest that for the specific boundary conditions studied by them no stationary two-dimensional flows may exist.

Yao (1978) has presented the most lucid outline of the physics of the flow in the entrance region of heated, circular pipes. He has shown the entry flow to depend on the following parameters: (*a*) Reynolds number, $Re = \langle v_z \rangle a/\nu$, (*b*) Grashof number, $Gr = \beta g a^4 q_w/k\nu^2$, (*c*) Prandtl number, $Pr = \nu/\kappa$, and (*d*) the ratio $\epsilon = Gr/Re^{2.5}$ where $\langle v_z \rangle$ is the average inlet velocity, a the pipe radius, ν the kinematic viscosity, β the coefficient of expansion, g the acceleration due to gravity, q_w the constant axial heat flux at the wall, k the thermal conductivity and κ the thermal diffusivity. Depending on the relative magnitude of the parameters, the interaction between the inviscid core, the axial boundary layer and the secondary boundary layer can take place over different length-scales. Yao (1978) identifies four such cases. The perturbation expansion solution developed by Yao (1978) is valid, however, only over a distance of $O(a)$ as the nonlinear interaction further downstream is highly complicated and is intractable by analytical means.

In a fully elliptic formulation the second-order diffusive terms in the predominant flow direction z are retained. Hence, a far downstream boundary condition is required to be specified. Typically this is specified as the fully developed state, *i.e.* gradients of velocities in the axial direction vanish. This of course restricts the possible solutions to those that evolve to a fully developed state. As pointed out earlier, streamwise-periodic, three-dimensional stationary solutions are known in the Dean problem. They have been computed in finite geometry by Ravi Sankar *et al.* (1988) and for infinite geometry by Finlay, Keller & Ferziger (1988). Because of the close analogy between the two problems we expect similar behaviour in the present problem.

A parabolized formulation entails neglecting the axial momentum diffusion in comparison to axial convection and is akin to the standard boundary-layer approximation. In flow situations where there is a predominant flow direction and no abrupt change in curvature of the geometry, this formulation has proven to be useful in predicting

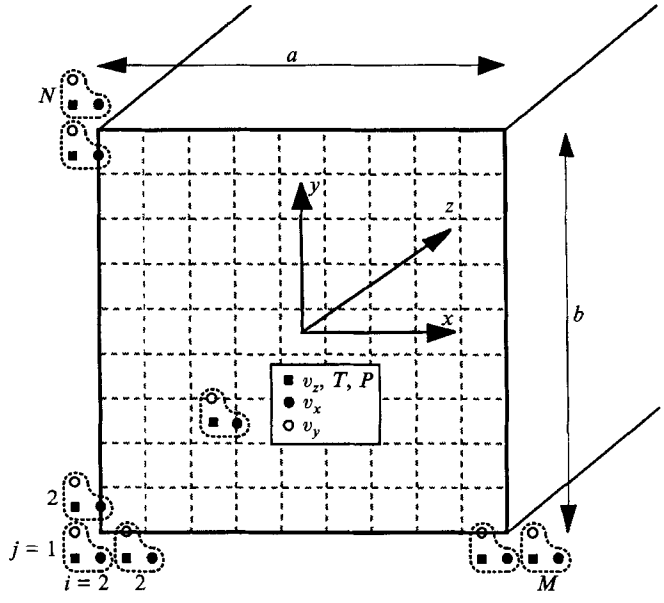

FIGURE 1. Geometry, coordinate system and grid layout

the flow development without excessive computing requirements. Bara *et al.* (1992) have validated the parabolized formulation for the Dean problem by comparing experimentally measured velocity profiles in the entrance region with those predicted by the parabolized model. Since the present geometry does not have any curvature on the streamwise direction, there is no possibility of streamwise flow reversals and hence the parabolized formulation should be equally valid for the Morton problem. We will show that it accurately tracks the flow and temperature development in the entrance region by comparing with literature values for the case of forced convection for which such results are available. In cases where it evolves into a fully developed state, the results once again agree with previously established values. For the streamwise-periodic flows grid sensitivity tests will indicate that such a phenomenon is not a numerical artifact. Another advantage of the parabolized formulation is that the wavelength in the streamwise direction is selected naturally by the marching scheme during the course of the flow evolution in the streamwise spatial direction. The wavelength so selected is insensitive to grid refinement, particularly the marching step size. In a fully elliptic formulation, however, a wavelength (or the length of the computational box in the streamwise direction) must be specified *a priori* and periodicity conditions must be imposed on the inflow and outflow boundaries.

2. Governing equations

The equations of motion, in the Cartesian coordinate system (figure 1), are parabolized by neglecting the axial (z-direction) momentum diffusion and the axial conduction and assuming that the variation of axial pressure gradient at a cross-plane is small while considering the axial momentum equation. The latter condition implies decomposing the pressure as $p'(x, y, z) = p'_m(z) + \bar{p}'(x, y)$. The equations are rendered dimensionless using the following scales:

$$\boldsymbol{x} = \boldsymbol{x}'/De', \qquad \boldsymbol{v} = \boldsymbol{v}'/(\nu/De'), \qquad p = p'/(\rho v^2/De'^2), \qquad T = (T'-T'_e)/(Q'De'/kP'),$$

where the prime denotes a dimensional quantity, $\boldsymbol{x} = (x, y, z)$ and $\boldsymbol{v} = (v_x, v_y, v_z)$ are the position and velocity vectors respectively, De' is the equivalent diameter, p' is the pressure, T_e' is the inlet temperature, Q' is the heat transfer rate per unit length in the axial z' direction, k is the thermal conductivity of the fluid and P' is the perimeter of the duct. The non-dimensionalized forms of the equations are:

Continuity equation

$$\frac{\partial v_x}{\partial x} + \frac{\partial v_y}{\partial y} + \frac{\partial v_z}{\partial z} = 0, \tag{2.1}$$

x–momentum equation

$$[\boldsymbol{v} \cdot \nabla] v_x = -\frac{\partial p}{\partial x} + \Delta v_x, \tag{2.2}$$

y–momentum equation

$$[\boldsymbol{v} \cdot \nabla] v_y = -\frac{\partial p}{\partial y} + \Delta v_y + 2\ Gr\ T, \tag{2.3}$$

z–momentum equation

$$[\boldsymbol{v} \cdot \nabla] v_z = -\frac{\mathrm{d}p_m}{\mathrm{d}z} + \Delta v_z, \tag{2.4}$$

Energy equation

$$Pr[\boldsymbol{v} \cdot \nabla] T = \Delta T, \tag{2.5}$$

Global continuity constraint

$$\int v_z \mathrm{d}x\ \mathrm{d}y = A\ Re, \tag{2.6}$$

Global energy balance

$$\oint \frac{\partial T}{\partial n} \mathrm{d}\xi = P, \tag{2.7}$$

$$\frac{RePr}{4} \frac{\mathrm{d}T_b}{\mathrm{d}z} = 1, \tag{2.8}$$

where

$$\Delta = \left[\frac{\partial^2}{\partial x^2} + \frac{\partial^2}{\partial y^2}\right], \qquad [\boldsymbol{v} \cdot \nabla] = \left[v_x \frac{\partial}{\partial x} + v_y \frac{\partial}{\partial y} + v_z \frac{\partial}{\partial z}\right], \qquad Gr = \frac{g\beta(Q'/P')De'^4}{kv^2},$$

and $Pr = [C_p \mu / k]$, $Re = [De' \langle v_z' \rangle / v]$. $A(=1)$ and $P(=4)$ are the cross-sectional area and perimeter of the duct and have the numerical values shown in parenthesis. The left-hand side of (2.7) represents the heat flux integrated around the periphery, ξ. The bulk temperature, T_b, in (2.8) is defined as the mixing cup temperature by

$$T_b = \frac{\int v_z\ T\ \mathrm{d}x\ \mathrm{d}y}{\int v_z\ \mathrm{d}x\ \mathrm{d}y}.$$

Note that the Reynolds number (forced flow parameter) appears explicitly only in (2.6) and (2.8) and a further transformation $z^* = z/Re$, $v_z^* = v_z/Re$, $p_m^* = p_m/Re^2$ leaves (2.1)–(2.5) unchanged and removes Re from (2.6) and (2.8). Thus the role of Re is merely to stretch the development length in the z direction. This was also

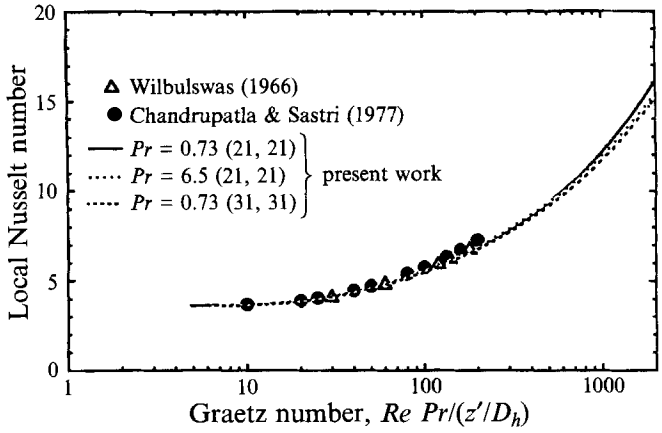

FIGURE 2. Peripherally averaged Nusselt number variation along the duct length for the limiting case of $Gr = 0$. Grid sensitivity test shows good agreement over the development length.

observed empirically by Mahaney *et al.* (1987). This observation is valid only in the context of a parabolized formulation and is an artifact to that extent. In an experimental realization of this problem, the duct geometry must necessarily be of finite *axial* length. Very near the inlet and exit the axial diffusion terms (the elliptic effect) will be important over a dimensionless axial distance $O(1/Re^2)$ (Hishida *et al.* 1982). It should be noted that in closed flow systems such as the convection box (*Rayleigh–Bénard* problem) or *Taylor–Couette* flow it is well known (Benjamin & Mullin 1982; Daniels 1981) that the end effects are felt through out the flow domain. In contrast, in open channel flows with a predominant flow direction, the effect of at least the downstream end condition could be confined to a small distance near the exit. The inlet condition of course will be *convected* into the observational domain and it becomes important to have a good control over the inlet conditions in an experiment. The side conditions (in the x- and y-directions) will, of course, be felt throughout the flow domain even in open channel flows. The boundary conditions for the velocities are: (i) no-slip condition on the duct wall ($v_x = v_y = v_z = 0$) and (ii) uniform *or* fully developed square duct profile for v_z at the inlet.

Axially uniform flux and peripherally uniform temperature are imposed on the energy equation together with uniform inlet temperature ($T = 0$). The reflective symmetry about $x = 0$ that is inherent in (2.1)–(2.5) is normally (Mahaney *et al.* 1987; Hishida *et al.* 1982) imposed to reduce the computational domain by half. This, however, restricts the possible solutions to symmetric ones. Our experience with the Dean problem (Sankar, Nandakumar & Masliyah 1988) indicates that this symmetry is broken when streamwise-periodic modes develop. Hence imposing this symmetry will not allow streamwise-periodic flows to develop which is perhaps the reason that such solutions have not been reported in previous studies. In the present work, the equations are solved over the *full cross-section.* Macroscopic quantities of interest are computed as follows:

$$f\,Re = \frac{1}{2}\frac{\mathrm{d}p_m}{\mathrm{d}z}\frac{1}{\langle v_z\rangle}, \qquad Nu_l(z) = \frac{1}{(T_w - T_b)}, \tag{2.9}$$

where f is the Fanning friction factor and Nu_l is the peripherally averaged Nusselt number at an axial position.

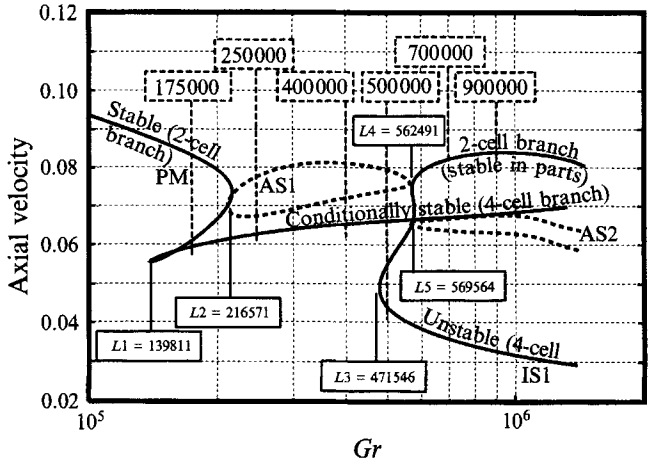

FIGURE 3. Bifurcation diagram of two-dimensional flows from I. In the window of Grashof numbers between $L2$ and $L3$ there are no unconditionally stable two-dimensional flows.

3. Numerical method

The governing equations were discretized by integrating them over a control volume. The resulting equations were solved using the SIMPLE algorithm as outlined by Patankar (1980). The mean pressure gradient, dp_m/dz, was determined by the secant method by satisfying the global continuity constraint (2.6). The wall temperature, T_w, was also determined by the secant method by satisfying the energy constraint (2.7). Equation (2.8) is used as further check on the energy balance at each axial position. In the limit of pure forced convection ($Gr = 0$) and fully developed flow, the (fRe, Nu) values changed from (14.117, 3.625) to (14.173, 3.618) as the grid was refined from 21×21 to 31×31 and both the results agree within 1% of published values of (14.227, 3.608) (Shah & London 1978). Excellent agreement in the developing region is also established by comparing the present Nu_l values with those of Wibulswas (1966) and Chandrupatla & Sastri (1977) as shown in figure 2 for two different grid sizes and Prandtl numbers. Additional evidence that the parabolized formulation can track the flow and temperature field development is to be found in Neti & Eichhorn (1983). They compare the numerical results with *experimental* data for the case of combined hydrodynamic and thermal development in a square duct using a numerical scheme very similar to the present one. They found a grid of 11×11 over one-quarter of the duct cross-section to be adequate and this agrees with our earlier observation that a grid of 21×21 over the full cross-section is adequate. Most of the simulations were done with an axial step size of $\Delta z = 0.0005$. Grid sensitivity studies were conducted for several values of Gr to ensure that the phenomena are not spurious artifacts of poorly resolved grids.

4. Results and discussion

Part of the bifurcation diagram for $Pr = 0.73$ and a square cross-section is reproduced from I in figure 3 for Grashof numbers in the range of $10^5 < Gr < 10^6$. The first limit point below which there is a unique two-dimensional solution occurs at $L1$ where $Gr = 139\,811$. The primary branch which has a two-cell flow structure remains unconditionally stable until the limit point $L2$ at $Gr = 216\,571$. An asymmetric solution branch originates at a symmetry breaking point near $L2$ and this branch

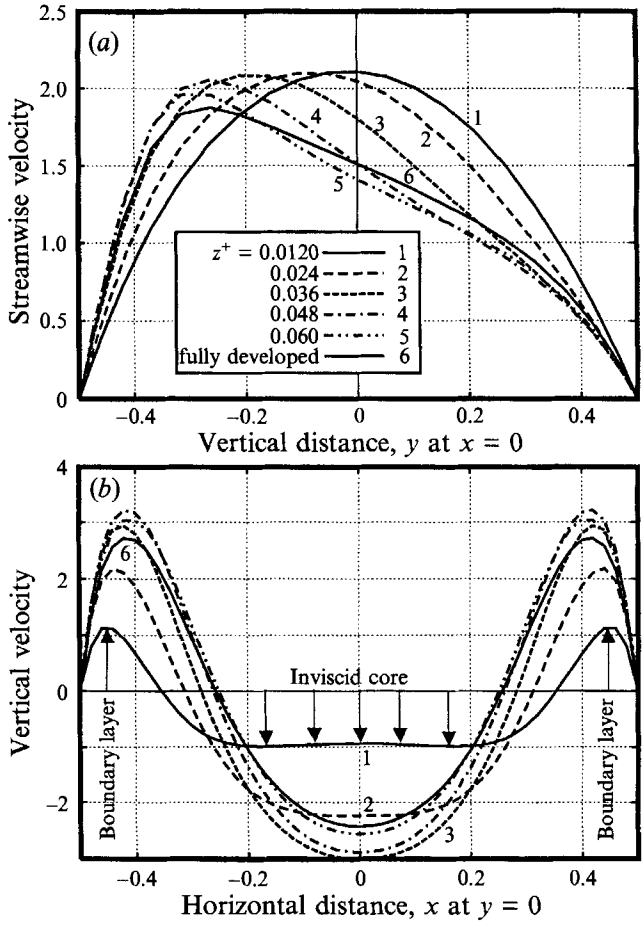

FIGURE 4. (*a*) Development of axial velocity, v_z, along the line of symmetry at various axial positions shows the evolution to a two-cell fully developed state for $Gr = 25000$, $Pr = 0.73$. (*b*) Vertical velocity at various axial positions shows the formation of boundary layers near the vertical walls and an inviscid core in the centre during early stages of secondary flow development.

is unstable. Between $L2$ and $L3$, the only symmetric solution that has been found has a four-cell flow structure and this solution branch is unstable to asymmetric perturbations. In what follows we present the results of a series of three-dimensional simulations at the Grashof numbers identified in figure 3. In each case the flow development is studied either from an initially parabolic (one-dimensional) inlet condition or from a fully developed, two-dimensional state subject to a specified inlet perturbation.

It is well known that in the fully developed region the secondary flow generated by the buoyancy force shifts the location of the maximum axial velocity away from the centre and in the direction in which the secondary flow is pointed, which is downwards in the present case. The evolution of the streamwise velocity component from an initially parabolic profile to a fully developed state is shown in figure 4(*a*) for $Gr = 25000$ and $Pr = 0.73$. At these parameter values there is a unique, two-dimensional solution with a two-cell pattern. The vertical velocity component is shown along $(x, y = 0)$ at various axial positions in figure 4(*b*). At short axial distances, the heating from the lateral boundaries results in a boundary-layer type

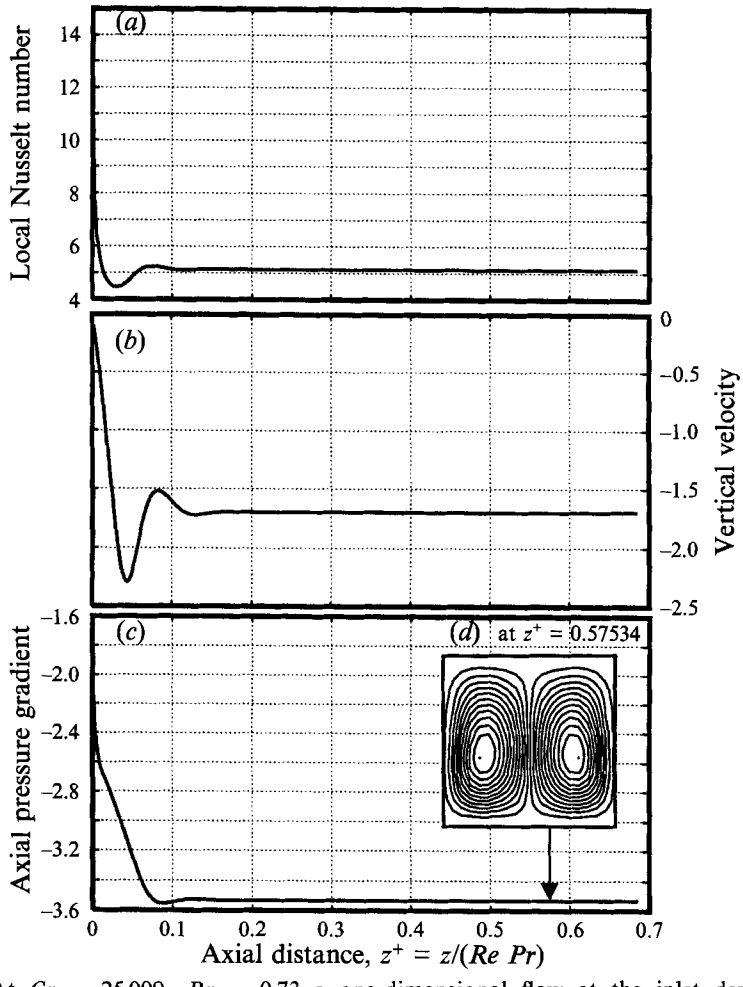

FIGURE 5. At $Gr = 25000$, $Pr = 0.73$ a one-dimensional flow at the inlet develops into a two-dimensional, two-cell flow. A 21×21 grid with $\delta z = 0.0025$ was used. (*a*) Peripherally averaged Nusselt number variation with z^+, (*b*) vertical velocity $v_y(0, -0.368)$ variation with z^+, (*c*) axial pressure gradient variation with z^+ and (*d*) Streamline contours in the fully developed region.

of upward flow near the vertical walls and this is accompanied by a bulk inviscid downward movement of the fluid near the centre. Such a model with an inviscid core and a secondary flow boundary layer has indeed been used in a number of earlier studies to develop approximate solutions to this class of problems – see for example Mori & Nakayama (1967). The viscous effects eventually penetrate to the centre of the duct. Note that throughout the development length, the expected symmetries about the vertical line $(x = 0, y)$ are preserved.

A fully developed state is reached at a dimensionless distance of $z^+ < 0.2$ as seen in figure 5, where (*a*) the peripherally averaged Nusselt number, $Nu_l(z^+)$, (*b*) the vertical velocity component $v_y(0, -0.368, z^+)$ and (*c*) the axial pressure gradient, $\mathrm{d}p_m/\mathrm{d}z$ are shown as a function of the axial position. The vertical velocity component at $(0, -0.368, z^+)$ is a sensitive indicator of any flow pattern changes. In the present case it is negative and reaches an invariant state, indicating that the flow has reached a fully developed two-cell state. A contour plot of the streamlines is shown in figure

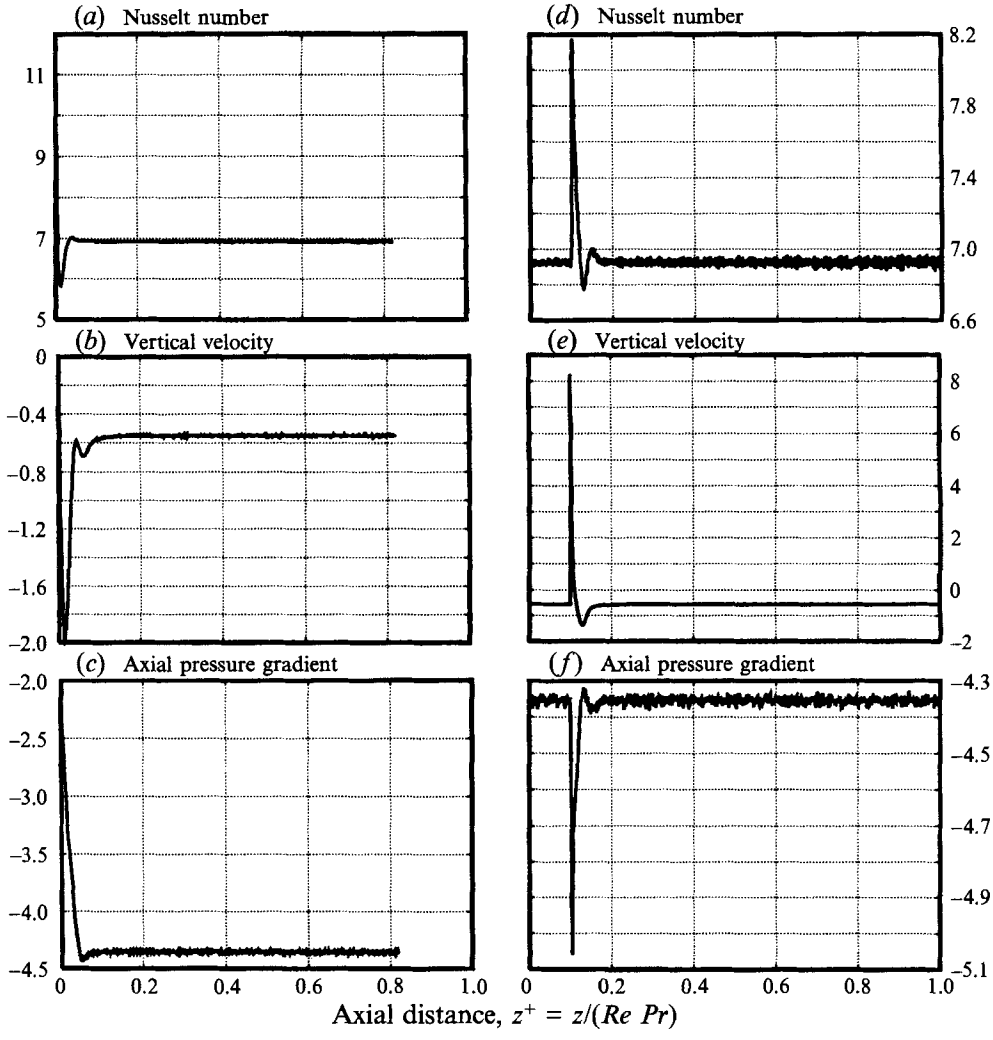

FIGURE 6. At $Gr = 175\,000$, which lies between $L1$ and $L2$ in figure 3, the fully developed two-cell flow remains stable. Hence the inlet flow should develop into that invariant state. (*a–c*) shows such a development from a one-dimensional inlet flow. In (*d–f*) the fully developed flow generated in (*a–c*) is perturbed at $z^+ = 0.1$; but the perturbation dies and the two-dimensional, two-cell flow is restored.

5(*d*). These are computed from the defining equations, $v_x = \partial\psi/\partial y$ and $v_y = -\partial\psi/\partial x$ which are of course valid only in the fully developed domain. The fully developed flow agrees well with our earlier two-dimensional computation in I.

A similar development pattern is seen in figure 6(*a–c*) for $Gr = 175\,000$. Note that this value of the Grashof number is still below $L2$ and hence there is an unconditionally stable, two-dimensional solution with a two-cell flow pattern. Hence a one-dimensional inlet velocity profile with a uniform temperature field evolves through a complex three-dimensional development region and reaches an invariant two-dimensional state at an axial position of about $z^+ \approx 0.15$.

Once such a two-dimensional flow has evolved, its stability can be probed by physically perturbing the flow by inserting a small needle at an appropriate axial

location. In experiments such tricks have been used (Masliyah 1980; Bara *et al.* 1992) to induce the development of four-cell flows. The objective, of course, is to provide a sufficiently large-amplitude perturbation to excite even those modes that have a small growth rate so that their effect can be realized over shorter duct lengths. We consider two such perturbations: (i) a symmetric one, in which the velocity components along $(x = 0, -0.5 \leqslant y \leqslant 0)$ at a specified axial position are set to zero and (ii) an asymmetric perturbation, in which the velocity components along $(x = -0.158, -0.5 \leqslant y \leqslant 0)$ are set to zero. These simulate insertion of a needle near the inlet, through the bottom wall of the duct either along the line of symmetry or away from the line of symmetry on one side only. The connection between this type of numerical experiment and the stability results of I are admittedly tenuous for the following reasons. The stability conclusions in I were based on a linear stability analysis of two-dimensional flows to two-dimensional perturbations only, while the proposed numerical experiment introduces a finite-amplitude perturbation and is inherently three-dimensional in nature. Nevertheless it provides useful information under at least two circumstances, viz. (i) when there is a stable two-dimensional solution on the primary branch, such a solution is restored even when it is subject to a finite-amplitude and possibly three-dimensional perturbation and (ii) in regions (such as between $L2$ and $L3$) where there are no stable two-dimensional solutions, the evolution of three-dimensional flows can be studied since the full nonlinear equations are subject to that perturbed flow field.

The two-dimensional solution shown in figure 6(*a–c*) was perturbed asymmetrically and the results shown in figure 6(*d, e*) indicate that the effect of such a perturbation decays rapidly and the symmetric, two-dimensional solution with a two-cell flow is restored for $Gr = 175\,000$. Similar tests at higher values of Gr show the flow to become convectively unstable and evolve in the downstream direction into completely new solutions.

The next simulation is for $Gr = 250\,000$ which is just past the limit point $L2$ and lies in the range of Gr where there are no stable two-dimensional solutions. Results of flow development from a one-dimensional inlet velocity field and a uniform temperature field are shown in figures 7–10. With such an inlet profile the initial stages $(0 < z^+ < 0.1)$ of the flow field development at any Gr follow essentially the same trend, viz. secondary flow (v_y) boundary layers develop near the vertical walls with the attendant inviscid downward displacement of fluid in the core as seen in figure 7(*b*). The streamwise velocity profile undergoes the characteristic shift in the direction of the body force which is left in figure 7(*a*). During this stage a strong secondary flow with two large cells are established and the flow field remains symmetric about the vertical centreline.

If such a flow is stable at that chosen Gr then it would reach an invariant state as found in the previous two cases. In the present case, however, there is no symmetric two-dimensional solution with a two-cell pattern. Hence the flow continues to develop over the range $0.1 < z^+ < 0.2$. Since there is a two-dimensional, four-cell flow at $Gr = 250\,000$ as seen in figure 3, the flow continues to evolve towards that state. During this stage also the flow field remains symmetric as seen in figure 7(*b*). Also, the secondary flow reversal near the centre of the duct indicates that a four-cell pattern is emerging. This switch from a two-cell to a four-cell pattern occurs over a short axial distance of $0.15 < z^+ < 0.2$. Figure 8 shows that such a four-cell flow retains its form including the symmetry over considerable axial length $(0.2 < z^+ < 0.5)$. But the stability results of I indicate that such a four-cell flow should be unstable to any asymmetric perturbations. This has some important implications for the observability

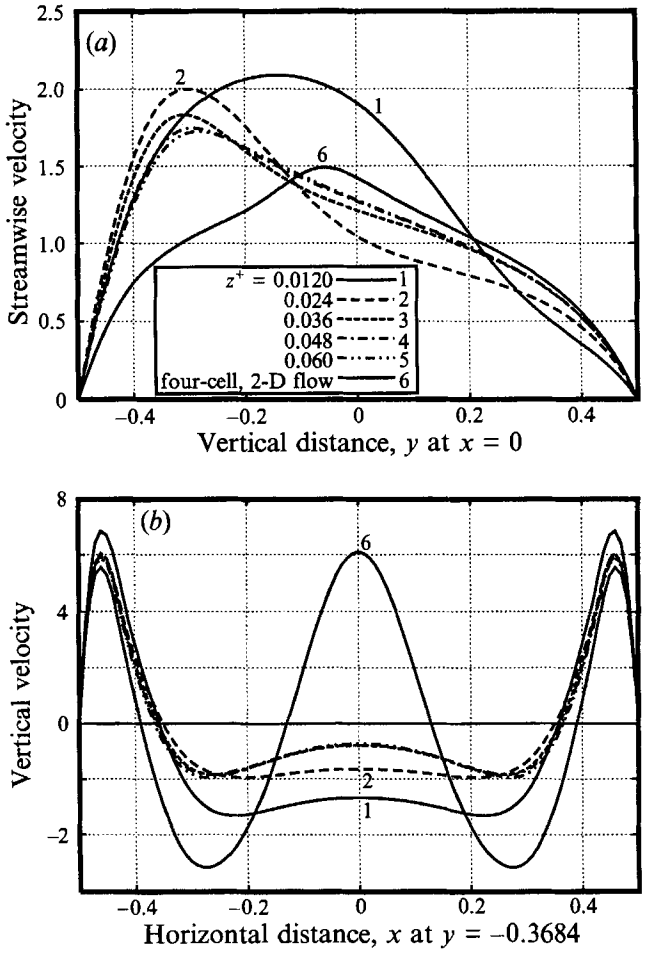

FIGURE 7. (*a*) Development of axial velocity, v_z, along the line of symmetry at various axial positions shows the evolution to a four-cell two-dimensional state over $z^+ \leqslant 0.4$ for $Gr = 250\,000$, $Pr = 0.73$. (*b*) Vertical velocity at various axial positions shows the formation of boundary layers near the vertical walls and a flow reversal in the core due to the formation of additional cells.

of such four-cell flows in experiments in spite of their predicted instability. The unstable asymmetric mode in such four-cell flows must have very slow growth rates for the four-cell flows to remain observable over long lengths of duct. The scenario outlined above has been verified experimentally by Bara *et al.* (1992) for the Dean problem which shares several common features with the Morton problem.

It should be pointed out that in the previous simulations no perturbations were imposed at the inlet and the computations were carried out in double precision. Thus any natural, random perturbations in the computations due to round off errors were kept to a minimum. Nevertheless, continuing the simulation over even larger lengths confirms that the four-cell flow is indeed unstable and a streamwise-periodic three-dimensional flow develops spontaneously beginning at $z^+ > 0.5$ as seen in figure 8. The projections of the velocity vector in the (x, z)-plane at various y locations are shown in figure 9. Similar projections in the (x, y)-plane are shown in figure 10 at various axial locations over one period. It is clear from these figures that most of the dynamic changes in the flow field occur in the lower half of the duct where the

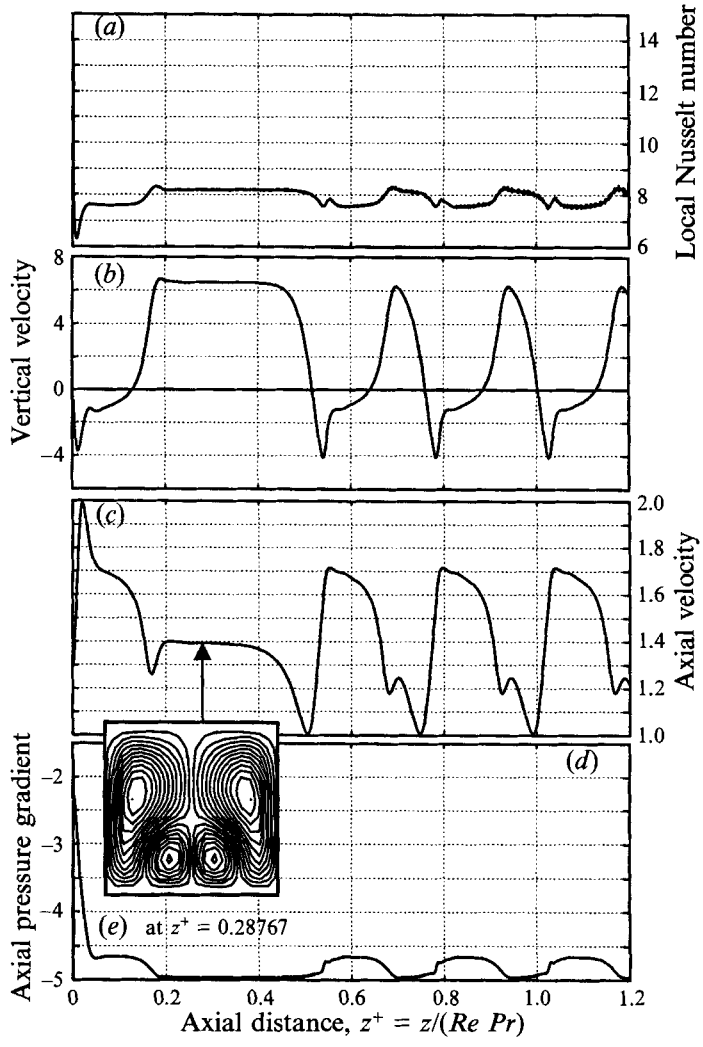

FIGURE 8. At $Gr = 250\,000$, which lies between $L2$ and $L3$ in figure 3, there are no stable two-dimensional solutions. (*a*) Peripherally averaged Nusselt number variation with z^+, (*b*) vertical velocity $v_y(0, -0.368)$ variation with z^+, (*c*) axial velocity $v_z(0, -0.368)$ variation with z^+, (*d*) axial pressure gradient variation with z^+ and (*e*) Streamline contours that correspond to the two-dimensional four-cell flows in the plateau region between $0.2 \leqslant z^+ \leqslant 0.4$. Since the two-dimensional, four-cell flow is unstable to asymmetric perturbations, the flow eventually develops a three-dimensional, streamwise-periodic structure.

temperature field is unstably stratified. Also the symmetry about the vertical centreline is destroyed and the secondary flow undergoes a sustained oscillation between a two-cell and a four-cell state. The additional two cells that are continuously formed and destroyed near the bottom of the duct roll over to one side (the left side in figure 10 and the upper side in figure 9*c*).

This new solution raises some interesting questions. The solution over one wavelength in the streamwise direction can be regarded as a solution that broke the continuous translational symmetry (*i.e.* two-dimensionality) in the z-direction into a discrete one while concurrently breaking the reflective symmetry about the vertical centreline ($x = 0, y$). The period of course has been selected naturally during the flow

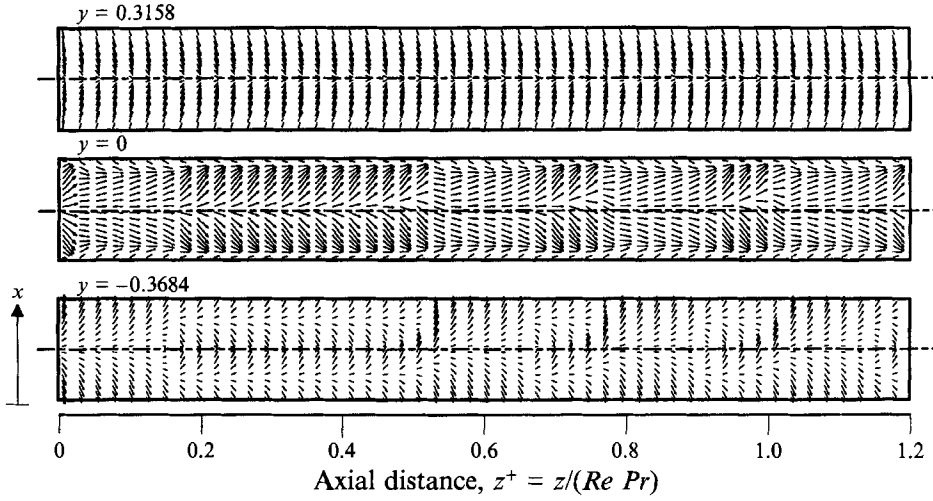

FIGURE 9. Projection of the velocity vectors in the (x, z)-plane elucidates the nature of the three-dimensional flow. The flow development remains symmetric until $z^+ \approx 0.5$. The symmetry is broken for $z^+ > 0.5$ and the flow oscillates between a two-cell and a four-cell structure with the destruction of the additional cells taking place in the positive x direction.

evolution. To establish that this is indeed a true three-dimensional, periodic solution to the problem and not a numerical artifact we must establish that (i) it does not in any way depend on the initial state from which it evolved and (ii) that it is insensitive to grid refinement tests. Breaking of the reflective symmetry about $(x = 0, y)$ also implies that this is an asymmetric, three-dimensional solution. Since the equations posses reflective symmetry, such asymmetric solutions must occur in pairs. Evidence in support of this is presented in figure 11(*a–e*) from two additional simulations at the same $Gr = 250\,000$. Starting with the same one-dimensional inlet profile as before, but using a grid of (31×31) in the cross-plane and $\delta z = 0.0005$ (which is a five-fold decrease in the axial step size) the flow evolves through the same stages as seen in figure 11(*a, b*). The wavelength changes from 0.243 to 0.251 which is about 3%, thus establishing grid insensitivity. Interestingly we have obtained the mirror image solution as seen in the vector plot of velocity projection in the (x, z)-plane in figure 11(*c*) and this choice in the flow evolution occurred spontaneously. This indicates that a three-dimensional solution branch must bifurcate from a two-dimensional branch through a pitch-fork bifurcation. The exact location of such symmetry-breaking points is beyond the scope of the present study.

In a variation of this simulation at the same $Gr = 250\,000$ and with the same inlet profiles, the flow was perturbed asymmetrically at an axial location of $z^+ = 0.1$. Results are shown in figure 11(*d, e*). Since this is a large-amplitude perturbation, it compensates for the slow growth rate of the four-cell mode and triggers the periodic mode almost immediately. The waveform and the period are not affected by the perturbation, indicating that these periodic solutions are independent of the initial state from which the flow evolves.

Results of additional tests, shown in figure 12, confirm the dual nature of the three-dimensional, asymmetric solutions. In this simulation a periodic state is established first in which the additional cells move downward in the (x, z)-projection (figure 12*c*) or right in the (x, y)-projection (figure 12*b*). Then the complete flow field corresponding to the state shown in figure 12(*b*) was flipped around the vertical

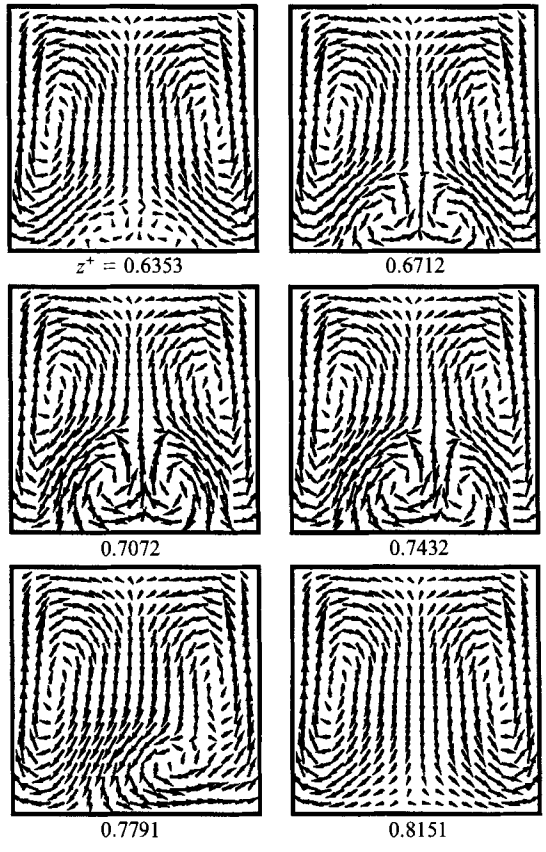

FIGURE 10. Projection of the velocity vectors in the (x, y)-plane is shown at various z^+ locations over one period in the streamwise direction. The formation and destruction of additional cells and the breaking of the reflective symmetry about the $x = 0$ axis are revealed clearly.

centreline $(x = 0, y)$ in accordance with the symmetry conditions as shown in figure 12(*d*) and it was used as the starting profile of the next simulation. The (x, z)-projection of the velocity field shown in figure 12(*f*) clearly confirms that the mirror image solution has been obtained. The horizontal velocity components v_x shown in figure 12(*a, e*) appear to be different because they were sampled at a point away from the line of symmetry, viz. (0.069, −0.3793).

Figure 13 shows, for $Gr = 400\,000$, $Pr = 0.73$, the flow development along the axial direction starting with a one-dimensional inlet profile. This point still lies in the window between $L2$ and $L3$ where there are no stable, two-dimensional solutions. The secondary flow development goes through the same phases as before, but with much more rapidity – the spontaneous switch to a periodic mode occurs around $z^+ \approx 0.35$ and the period has also decreased significantly to 0.146.

The next simulation is at $Gr = 500\,000$ which lies between $L3$ and $L4$. From figure 3 it can be seen that there are five two-dimensional solutions at this value of Gr, but none are stable. The results of the developing flow simulation starting from a one-dimensional inlet flow are shown in figure 14. The early stages of flow development are exactly the same as before, viz. two large cells form first followed by additional cells near the lower-centre part of the duct and the flow retains the symmetry until the axial distance of about $z^+ \approx 0.35$. This symmetry is spontaneously

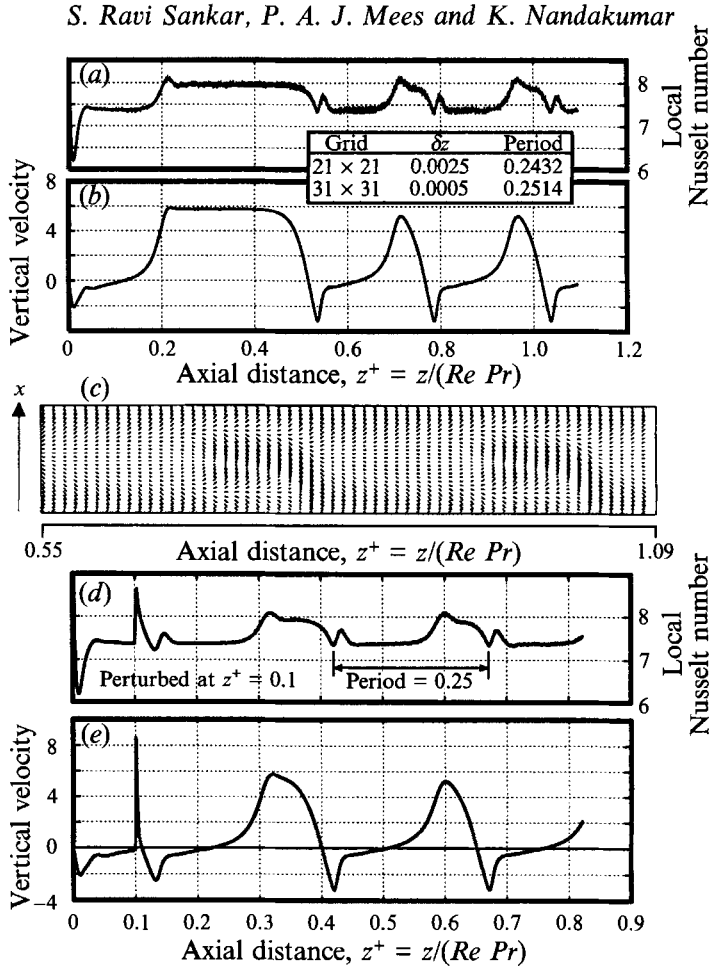

FIGURE 11. Grid sensitivity of streamwise periodic flows. (*a, b*) The same waveform and period are obtained upon refining the grid from 21 × 21 to 31 × 31 and δz from 0.0025 to 0.0005. (*c*) The velocity vector projection on the (x, z)-plane reveals the mirror image solution of the earlier one presented in figure 9. (*d, e*) A perturbation at $z^+ = 0.1$ simulating a needle insertion has no effect on the nature of the streamwise periodic flows.

broken further downstream and interestingly the additional cells are periodically destroyed and reformed on either side of the line of symmetry as seen in figure 14(*e*). Unlike the previous cases, the three-dimensional periodic solution obtained is a symmetric one. Note that quantities like peripherally averaged Nusselt number (figure 14*a*) or local values of velocity sampled on the line of symmetry (figure 14*d*) show half the period indicated in figure 14(*b*), while local quantities sampled away from the line of symmetry (figure 14*b, c*) show the true period to be 0.212. In a fully elliptic formulation, of course, one can take half the wavelength to be the length of the computational box in the streamwise direction and impose shift-and-reflect symmetry to generate solutions of this type directly. It should be pointed out that the results shown in figure 14 were obtained on a grid of 21 × 21 × 0.0025. As in all the previous cases, grid sensitivity was checked by repeating the simulation on a finer grid of 31 × 31 × 0.0005. Starting with an one-dimensional inlet profile, however, resulted in a periodic solution of the asymmetric type described earlier at other values

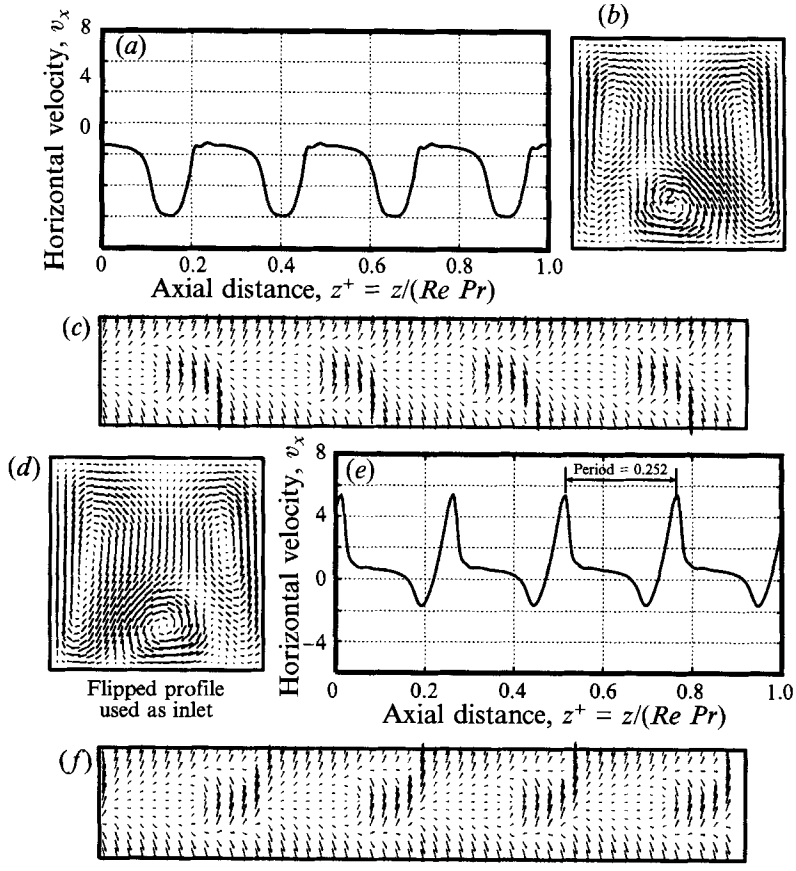

FIGURE 12. Dual, three-dimensional solutions at $Gr = 250000$, $Pr = 0.73$. (*a*) $v_x(0.069, -0.3793)$, (*b*) velocity vector projected on (x, y)-plane at $z^+ = 0.935$, (*c*) velocity vector projected on (x, z)-plane at $y = -0.4138$. (*d*) the profile shown in (*b*) is flipped and used as the inlet profile to obtain the mirror image solution. (*e*) $v_x(0.069, -0.3793)$ corresponds to the mirror image solution of (*a*); (*f*) velocity vector projected on (x, z)-plane at $y = -0.4138$ corresponds to the mirror image solution of (*c*).

of *Gr*. This raises some doubt about the validity of the symmetric, three-dimensional solution and warrants further investigation.

Some possible explanations are as follows: (i) both the symmetric and asymmetric type of three-dimensional flows might co-exist at $Gr = 500000$ and the region of attraction of each solution will then determine which one is realized in any physical or numerical experiment; (ii) there might be a singular point (either a limit point or a symmetry-breaking bifurcation point) of the three-dimensional solutions in this neighbourhood of *Gr*. Its location itself will be sensitive to changes in grid resolution and it might move past $Gr = 500000$ as the grid is refined from 21×21 to 31×31.

In an effort to shed additional light on this, several simulations were carried out. Keeping the cross-plane grid resolution the same at 21×21, the streamwise grid was refined from $\delta z = 0.0025$ to $\delta z = 0.0005$. This five-fold change in grid size did not change the flow structure. A three-dimensional, symmetric solution was reproduced and the period changed slightly from 0.212 to 0.208. Hence only the cross-plane resolution appears to have a crucial effect. The profile on the exit cross-plane that corresponds to the symmetric, three-dimensional solution was interpolated from a

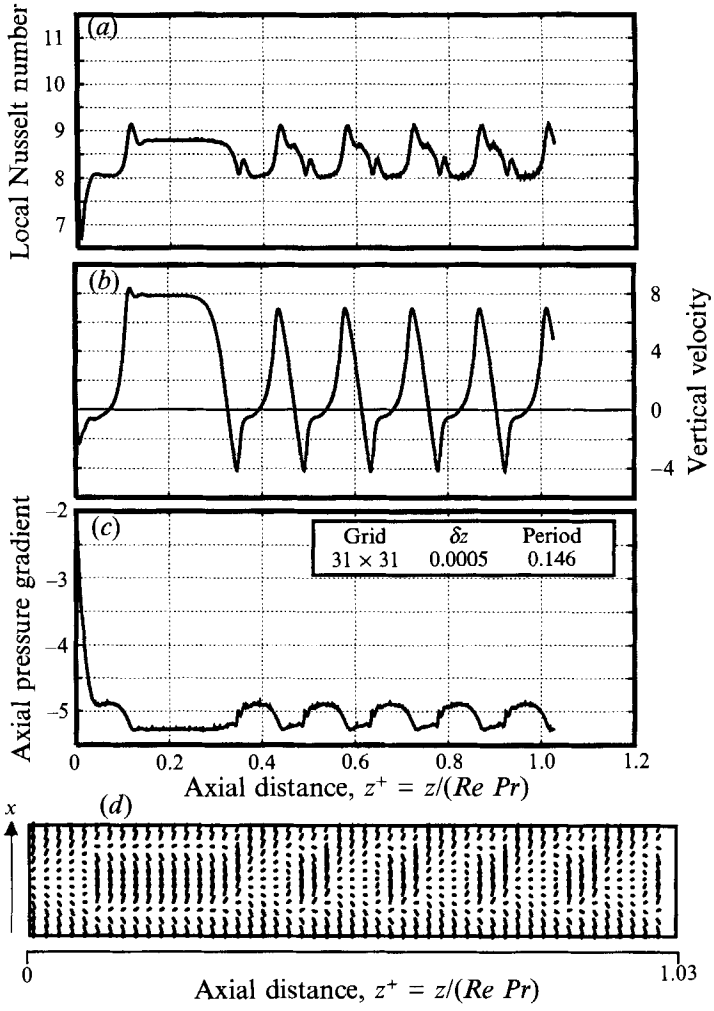

FIGURE 13. At $Gr = 400\,000$, which lies between $L2$ and $L3$ in figure 3, there are no stable two-dimensional solutions. (*a*) Peripherally averaged Nusselt number variation with z^+, (*b*) vertical velocity $v_y(0, -0.3793)$ variation with z^+, (*c*) axial pressure gradient variation with z^+ and (*d*) velocity vector projected on (x, z)-plane at $y = -0.4138$. Since the two-dimensional, four-cell flow is unstable to asymmetric perturbations, the flow eventually develops a three-dimensional, streamwise-periodic structure. The period decreases with increasing Gr.

21×21 grid to finer grids of up to 31×31 in an effort to remain within the region of attraction of the three-dimensional, symmetric solution. The flow pattern retained its symmetry on grids of up to 27×27, but switched to the asymmetric mode upon further grid refinement. Results of the symmetric solution on the 27×27 grid are shown in figure 15. This leads us to believe that the second conjecture above is the likely cause of this phenomenon. This cannot, however, be verified without a comprehensive bifurcation study of the three-dimensional flows.

Results of a final simulation at a heating rate corresponding to $Gr = 700\,000$ are shown in figure 16. This point lies above $L5$ in figure 3 and parts of this two-cell branch were found to be stable in I. It was shown in I that as the aspect ratio of the duct was increased, the limit points $L2$ and $L4$ approach each other and

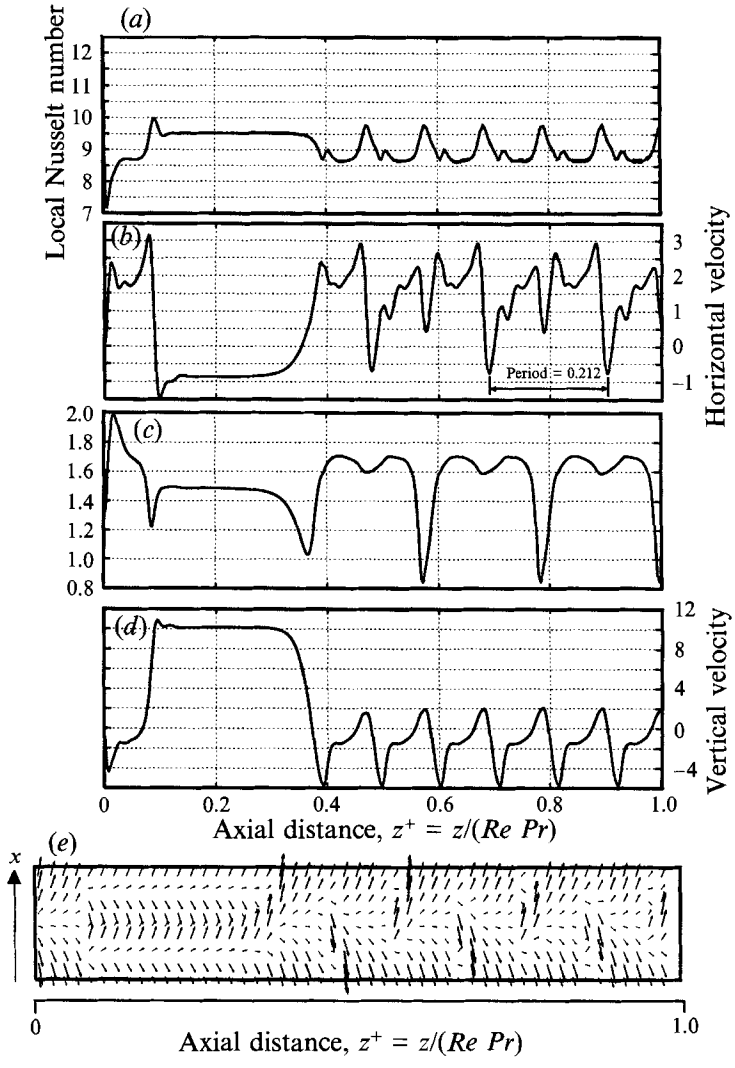

FIGURE 14. At $Gr = 500000$, which lies between $L3$ and $L4$ in figure 3, there are up to five two-dimensional solutions, but none are stable. (*a*) Peripherally averaged Nusselt number variation with z^+, (*b*) horizontal velocity $v_x(0.105, -0.316)$ variation with z^+, (*c*) axial velocity $v_z(0.105, -0.316)$ variation with z^+, (*d*) vertical velocity $v_y(0, -0.316)$ variation with z^+ and (*e*) velocity vector projected on (x, z)-plane at $y = -0.368$. The flow eventually develops a three-dimensional, streamwise-periodic structure, with the additional cells alternating on either side of the line of symmetry.

around an aspect ratio of 1.405, the two-cell branches merge through a transcritical bifurcation point. Hence we expect the same stability attribute on both parts of the two-cell branch. As a strong test of this expectation, the non-symmetric solution found at the exit for $Gr = 500000$ was used as the inlet condition for the simulation at $Gr = 700000$. Figure 16 clearly shows that a two-dimensional state is established within a short distance of $z^+ \approx 0.2$. Furthermore the reflective symmetry is restored even though the inlet profile was asymmetric. A similar simulation was carried out at $Gr = 900000$ with a similar result.

The results presented for Gr of up to 900000 are completely consistent with the known results from our earlier two-dimensional study and reveal several new features

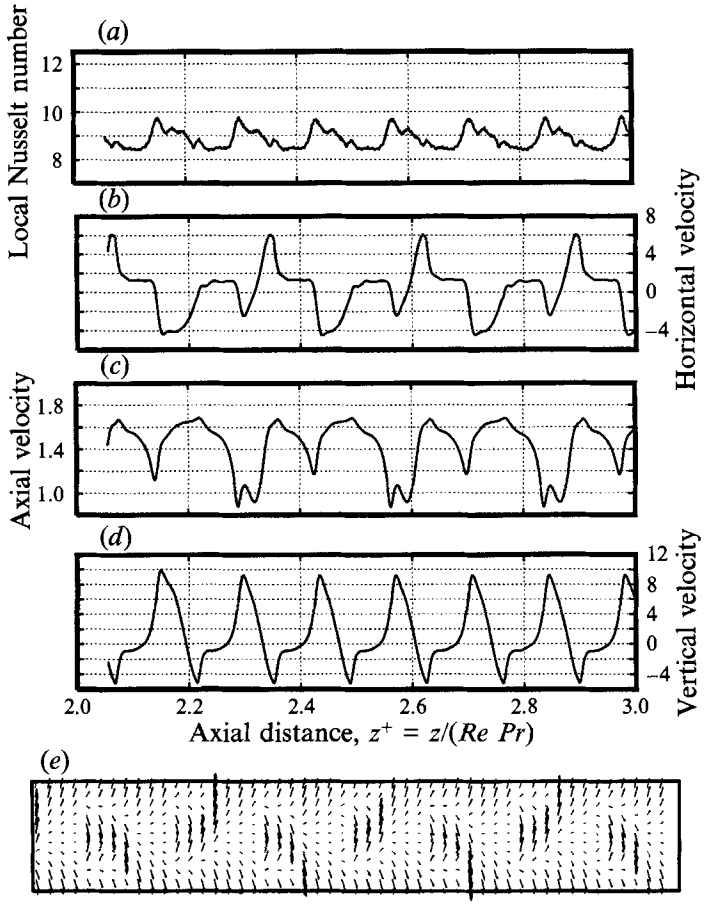

FIGURE 15. The profile from the exit state in figure 14 has been interpolated to a finer grid of 27×27 and used as the inlet profile. (*a*) Peripherally averaged Nusselt number variation with z^+, (*b*) horizontal velocity $v_x(0.080, -0.360)$ variation with z^+, (*c*) axial velocity $v_z(0.080, -0.360)$ variation with z^+, (*d*) vertical velocity $v_y(0, -0.360)$ variation with z^+ and (*e*) velocity vector projected on (x, z)-plane at $y = -0.400$.

of three-dimensional flows. We conclude with a few speculative thoughts as to how the flow might evolve at even higher values of Gr. Continuing with the same grid resolution and increasing the value of Gr we observed a spatially evolving chaotic flow with no discernible structure. Stability determination in I showed that at $Gr = 3 \times 10^6$ the two-cell branch was unstable. But no additional two-dimensional, stationary bifurcating solutions were found on this branch. It is likely that there are some Hopf bifurcation points on the two-cell branch at these high Grashof numbers, as some complex pairs of eigenvalues were computed in I. Although these might be valid singular points of the two-dimensional equations of motion, the two-dimensional, time-periodic flows that evolve at these locations are not physically realizable. We expect solutions that evolve both in space (in the streamwise direction) and in time. Travelling wave solutions are possible candidates. We believe that it is not fruitful to go beyond a Grashof number of over a million, without increasing the spatial resolution and more importantly including the time-varying formulation to capture any travelling wave phenomena. Hence any future work on the Morton problem should focus on constructing the complete bifurcation diagram of three-dimensional,

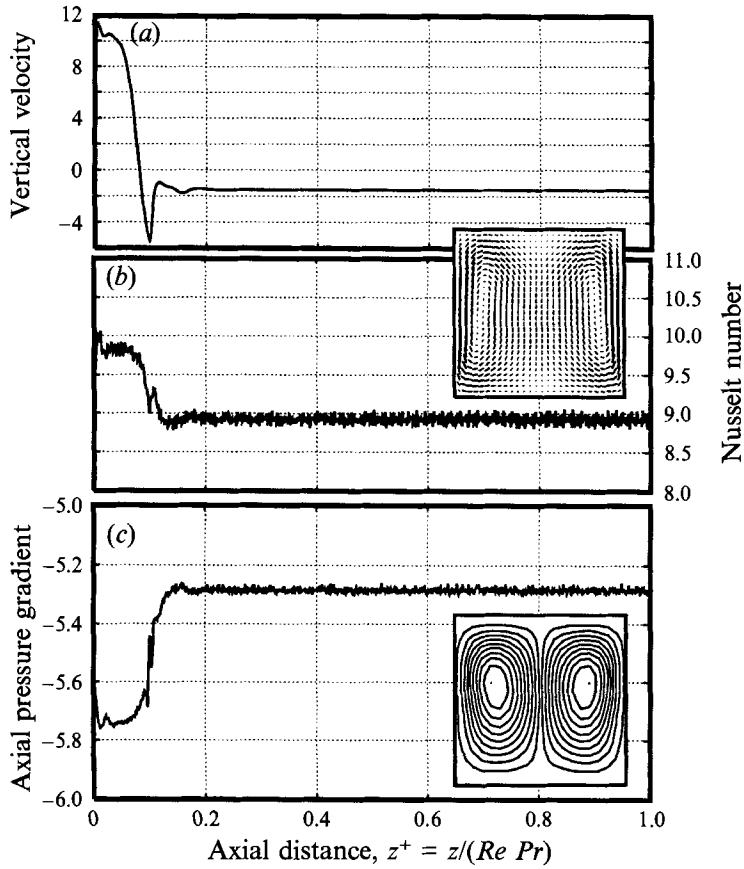

FIGURE 16. At $Gr = 700\,000$ there is a stable two-dimensional solution with a two-cell flow structure. Hence starting with even a nonsymmetric, three-dimensional profile that was obtained on a $31 \times 31 \times 0.0005$ grid for $Gr = 500\,000$ as the inlet profile and increasing Gr to 700 000 results in the quick destruction of the non-symmetric flow. A two-dimensional flow with a two-cell profile is re-established. Note that the reflective symmetry is also restored.

stationary flows and on simulating both the spatial and temporal evolution of flows at higher heating rates.

The effect of Prandtl number on the flow development was also investigated in the present study. Values of $Pr = 0.73$ and 6.5 correspond very nearly to that of air and water respectively. As shown in I, the bifurcation structure of the two-dimensional flows was unchanged over this range of Pr; but the singular points occurred at lower values of Gr as the Prandtl number was increased. The development of three-dimensional flows at $Pr = 6.5$ followed essentially the same pattern as for $Pr = 0.73$. Hence these results are not presented in detail.

5. Conclusions

A parabolized form of the equations of motion and energy has been shown to track the flow development in the entrance region quite accurately. For the case of axially uniform heat flux, which provides a sustained forcing, the flow development pattern follows closely that in the Dean problem. At low values of Gr, where a unique two-cell state exists in the fully developed region, any type of inlet perturbation

decays rapidly. Over an intermediate range of Gr, where multiple two-dimensional states were shown to exist in I, a one-dimensional flow at the inlet evolves through a complex transition zone into a streamwise-periodic, three-dimensional flow. In the transition zone, a two-cell structure forms first followed by the development of two additional cells. They remain symmetric and almost invariant over sufficiently long lengths of the duct. Such flows are, however, unstable and hence they eventually develop asymmetries and evolve into the streamwise-periodic flows. Some of these three-dimensional solutions do not conform to the symmetry properties expected of the equations; hence they occur in multiplicities of two. The streamwise wavelength, selected naturally by the marching scheme, is insensitive to grid refinement. The wavelength decreases with increasing Grashof number. Results obtained from the parabolized three-dimensional equations are completely consistent with the known stability and multiplicity results of two-dimensional flows.

It is believed that the two-dimensional four-cell flows are experimentally observable mainly because the growth rate of the asymmetric modes in the axial direction are small at lower values of Gr. At a higher Gr any type of inlet perturbation decays and a two-cell state is recovered downstream. In spite of the parabolization, the three-dimensional simulations are still CPU intensive and hence no attempt has been made to bracket the critical values of the parameters at which three-dimensional flows bifurcate from two-dimensional ones. At Grashof numbers larger than the values covered here, we expect the time-dependent behaviour to become important. We have focused here only on stationary solutions.

This work was supported in part through an operating grant from the Natural Sciences and Engineering Research Council of Canada. The early part of this work was carried out while K.N. was on a Humboldt research fellowship which is also gratefully acknowledged.

REFERENCES

ABOU-ELLAIL, M. M. M. & MORCOS, S. M. 1983 Buoyancy effects in the entrance region of horizontal rectangular channels. *Trans. ASME* C: *J. Heat Transfer* **105**, 924–928.

BARA, B., NANDAKUMAR, K. & MASLIYAH, J. H. 1992 An experimental and numerical study of the Dean problem: flow development towards two-dimensional multiple solutions. *J. Fluid Mech.* **244**, 339–376.

BENJAMIN, T. B. & MULLIN, T. 1982 Notes on the multiplicity of flows in the Taylor experiment. *J. Fluid Mech.* **121**, 219–230.

BERGLES, A. E. & SIMONDS, R. R. 1971 Combined forced and free convection for laminar flow in horizontal tubes with uniform flux. *Intl J. Heat Mass Transfer* **14**, 1989–2000.

BRILEY, W. R. 1971 Numerical method for predicting three-dimensional steady viscous flow in ducts. *J. Comput. Phys.* **14**, 8–28.

CHANDRUPATLA, A. R. & SASTRI, V. M. K. 1977 Laminar forced convection heat transfer of non-Newtonian fluid in a square duct. *Intl J. Heat Mass Transfer* **20**, 1315–1324.

CHOU, F. C. & HWANG, G.-J. 1984 Combined free and forced laminar convection in horizontal rectangular channels for high Re-Ra. *Can. J. Chem. Engng* **62**, 830–836.

DANIELS, P. G. 1981 The effect of distant side-walls on the evolution and stability of finite-amplitude Rayleigh-Bénard convection. *Proc. R. Soc. Lond.* A **378**, 539–566.

DENNIS, S. R. C. & NG, M. 1982 Dual solutions for steady laminar flow through a curved tube. *Q. J. Mech. Appl. Maths* **35**, 305–324.

FINLAY, W. H., KELLER, J. B. & FERZIGER, J. H. 1988 Instability and transition in curved channel flow. *J. Fluid Mech.* **194**, 417–456.

FUNG, L., NANDAKUMAR, K. & MASLIYAH, J. H. 1977 Bifurcation phenomena and cellular-pattern evolution in mixed-convection heat transfer. *J. Fluid Mech.* **177**, 339–357.

HIEBER, C. A. & SREENIVASAN, S. K. 1974 Mixed convection in an isothermally heated horizontal pipe. *Intl J. Heat Mass Transfer* **17**, 1337–1348.

HISHIDA, M., NAGANO, Y. & MONTESCLAROS, M. S. 1982 Combined forced and free convection in the entrance region of an isothermally heated horizontal pipe. *Trans. ASME* C: *J. Heat Transfer* **104**, 153–159.

INCROPERA, F. P. & SCHUTT, J. A. 1985 Numerical simulation of laminar mixed convection in the entrance region of horizontal rectangular ducts. *Numer. Heat Transfer* **8**, 707–729.

MAHANEY, H. V., INCROPERA, F. P. & RAMADHYANI, S. 1987 Development of laminar mixed convection flow in a horizontal rectangular duct with uniform bottom heating. *Numer. Heat Transfer* **12**, 137–155.

MASLIYAH, J. H. 1980 On laminar flow in curved semicircular ducts. *J. Fluid Mech.* **99**, 469–479.

MONKEWITZ, P. A. 1990 The role of absolute and convective instability in predicting the behavior of fluid systems. *Eur. J. Mech.* B/*Fluids* **9**, 395–413.

MORI, Y. & NAKAYAMA, W. 1967 Forced convective heat transfer in a straight pipe rotating about a parallel axis (Laminar region). *Intl J. Heat Mass Transfer* **10**, 1179–1194.

MORTON, B. R. 1959 Laminar convection in uniformly heated horizontal pipes at low Rayleigh numbers. *Q. J. Mech. Appl. Maths* **12**, 410–420.

NANDAKUMAR, K. & MASLIYAH, J. H. 1982 Bifurcation in steady laminar flow through curved tubes. *J. Fluid Mech.* **119**, 475–490.

NANDAKUMAR, K., MASLIYAH, J. H. & LAW, H.-S. 1985 Bifurcation in steady laminar mixed convection flow in horizontal ducts. *J. Fluid Mech.* **152**, 145–161.

NANDAKUMAR, K. & WEINITSCHKE, H. J. 1991 A bifurcation study of mixed convection heat transfer in horizontal ducts. *J. Fluid Mech.* **231**, 157–187 (referred to herein as I).

NETI, S. & EICHHORN, R. 1983 Combined hydrodynamic and thermal development in a square duct. *Numer. Heat Transfer* **6**, 497–510.

OSBORNE, D. G. & INCROPERA, F. P. 1985 Laminar, mixed convection heat transfer for flow between horizontal parallel plates with asymmetric heating. *Intl J. Heat Mass Transfer* **28**, 207–217.

PATANKAR, S. V. 1980 *Numerical Heat Transfer and Fluid Flow.* McGraw Hill.

PATANKAR, S. V., RAMADHYANI, S. & SPARROW, E. M. 1978 Effect of circumferentially nonuniform heating on laminar combined convection in a horizontal tube. *Trans. ASME* C: *J. Heat Transfer* **100**, 63–70.

SANKAR, S. R., NANDAKUMAR, K. & MASLIYAH, J. H. 1988 Oscillatory flows in coiled square ducts. *Phys. Fluids* **31**, 1348–1358.

SHAH, R. K. & LONDON, A. L. 1978 Laminar flow forced convection in ducts. In: *Advances in Heat Transfer.* Academic.

VAN DYKE, M. 1990 Extended Stokes series: laminar flow through a heated horizontal pipe. *J. Fluid Mech.* **212**, 289–308.

WIBULSWAS, P. 1966 Laminar flow heat transfer in ducts of rectangular cross-section. Ph.D. thesis, London University, London.

WINTERS, K. H. 1987 A bifurcation study of laminar flow in a curved tube of rectangular cross-section. *J. Fluid Mech.* **180**, 343–369.

YAO, L.-S. 1978 Entry flow in heated straight tube. *J. Fluid Mech.* **88**, 465–483.

YOUSEF, W. W. & TARASUK, J. D. 1981 An interferometric study of combined free and forced convection in a horizontal isothermal tube. *Trans. ASME* C: *J. Heat Transfer* **103**, 249–256.